return of MeNC or t-BuNC at low viscosities were observed. Such reactions should also show an inversion of $\Delta V^{\ddagger}$. These and other near diffusion controlled reactions are under study both to clarify their reaction mechanisms and to probe the generality of this pressure-viscosity method.

Acknowledgment. Studies at U.C. Santa Barbara were supported by grants to P.C.F. from the National Science Foundation (CHE 87-22561 and CHE 90-24845). Studies at U.C. San Diego were supported by grants from National Institutes of Health (PHS HL 13581).

Registry No. CO, 630-08-0; MCPH-CO, 140361-24-6; protoheme-3-(1-imidazolyl)propylamide methyl ester chloride, 72177-42-5.

Molecular and Electronic Structures of Pentaammineruthenium(II)-Thioether Complexes. The Nature of Ru(II)-S Back-Bonding Elucidated by Structural, Electronic Spectral, and Molecular Orbital Studies

Karsten Krogh-Jespersen,* Xiaohua Zhang, Yanbo Ding, John D. Westbrook, Joseph A. Potenza,* and Harvey J. Schugar*

Contribution from the Department of Chemistry, Rutgers, The State University of New Jersey, New Brunswick, New Jersey 08903. *Received November 4, 1991*

Abstract: The nature of Ru(II)-S(thioether) bonding has been probed by a combination of structural, spectroscopic, and computational methods. The synthesis, X-ray structure, and electronic spectra are presented for the $(NH_3)_5Ru[S(CH_3)(C_2H_5)]\cdot 2PF_6$ complex which crystallizes in the monoclinic space group $P2_1/n$ with $a = 8.3664$ (5) Å, $b = 12.337$ (1) Å, $c = 17.780$ (1) Å, $\beta = 100.388$ (5)°, $V = 1805.1$ (4) Å^3, $Z = 4$, and $R_F(R_{wF}) = 0.042$ (0.072) for 3475 reflections. The structure contains approximately octahedral $(NH_3)_5RuS(Me)Et^{2+}$ cations separated by disordered PF_6^- anions. The Ru(II)-N distances span the range 2.135 (4)-2.168 (4) Å and average 0.043 Å longer than those of the Ru(III) analogue. In contrast, the Ru(II)-S distance of 2.316 (1) Å is 0.055 Å shorter than that of the Ru(III) analogue, implying substantial back bonding. Structural parameters of the coordinated thioether in both Ru(II)- and Ru(III)-thioether complexes are close to those reported for the free ligand. Ab initio molecular orbital (MO) calculations have been performed on the ground state of the $(NH_3)_5Ru^{II}S(CH_3)_2$ complex with full geometry optimizations carried out at the Hartree-Fock (HF) level; partial geometry optimizations were made with correlation energy corrections included via Moller-Plesset perturbation theory (MP2, MP3). Good agreement between calculated and experimental structures is obtained only at the correlated (MP2, MP3) levels; at the HF level, the Ru(II)-S distance is computed more than 0.2 Å too long. Electronic population analyses at both the HF and MP2 levels are used to elucidate the metal-thioether interactions, in particular with respect to the nature of Ru(II)-S back bonding. Semiempirical MO calculations (INDO/S) using singly excited configuration interaction (SECI) and time-dependent Hartree-Fock (TDHF) methods permit assignment of the electronic spectra. Two Ru-thioether MLCT transitions are located in the 35 000-40 000-cm^{-1} region; in addition, a LMCT transition occurs at slightly higher energy (~45 000 cm^{-1}).

Introduction

Structural parameters and properties of the kinetically stable six-coordinate $(NH_3)_5Ru^{II}L$ and $(NH_3)_5Ru^{III}L$ complexes reflect electronic interactions of the ligand L with the metal d-orbitals. It is well-known that the electron rich t_{2g}^6 $(NH_3)_5Ru^{II}L$ complexes are preferentially stabilized if L is a π-acceptor and that the t_{2g}^5 $(NH_3)_5Ru^{III}L$ complexes, having a vacancy in the metal ion t_{2g} level, are stabilized when L is a π-donor. This ligand dependency of complex stability has been quantitated by extensive electrochemical studies of the Ru(II)/Ru(III) redox potentials in such systems.[1-3] The range of ligand π-acceptors to π-donors has been varied from N_2 to OH^-, and the resulting changes in redox potentials span 1.5 V.[3] Ligands may be ranked according to their affinities[3] for Ru(II) or Ru(III) and in an electrochemical series[4] according to their π-accepting/donating behavior.

Structural consequences of these π-bonding effects have been the subject of several crystallographic studies. When L is a π-acceptor such as pyrazine[5] or *N*-methylpyrazinium,[6] the Ru(II)-L bond distances are 0.07 or 0.13 Å shorter than the corresponding Ru(III)-L distances. In contrast, the Ru(II)-NH_3 bonds involving the purely σ-donating ammine ligands average about 0.03 Å longer than the Ru(III)-NH_3 bonds. Combined structural, spectroscopic, and computational studies of the $(NH_3)_5Ru^{III}L$ system in which L = imidazole (histidine) indicated that the strong σ-donor/weak π-donor nature of imidazole was responsible for the Ru(III)-imidazole bond being even shorter than the Ru(III)-N bonds to the above types of heterocyclic π-acceptor ligands.[7]

There has been considerable interest in the systems for which L = thioether. Thioether preferentially binds to and stabilizes the $(NH_3)_5Ru^{II}$ unit.[1] The resulting increase in the Ru(II) oxidation potential is comparable to that achieved by π-acceptor ligands such as pyridine, phosphine, or nitrile.[1,2,4] The kinetic stabilities of both the Ru(II)- and Ru(III)-thioether bonds allow the synthesis of mixed-valence systems with $(NH_3)_5Ru^{II,III}$ units linked by variable length oligospirocyclobutanes terminated by ligating thietanes.[8-12] These weakly coupled metal ion chro-

(1) Kuehn, C. G.; Taube, H. *J. Am. Chem. Soc.* **1976**, *98*, 689.
(2) Matsubara, T.; Ford, P. C. *Inorg. Chem.* **1976**, *15*, 1107.
(3) Lim, H. S.; Barclay, D. J.; Anson, F. C. *Inorg. Chem.* **1972**, *11*, 1460.
(4) Lever, A. B. P. *Inorg. Chem.* **1990**, *29*, 1271.
(5) Gress, M. E.; Creutz, C.; Quicksall, C. O. *Inorg. Chem.* **1981**, *20*, 1522.
(6) Wishart, J. F.; Bino, A.; Taube, H. *Inorg. Chem.* **1986**, *25*, 3318.
(7) Krogh-Jespersen, K.; Westbrook, J. D.; Potenza, J. A.; Schugar, H. J. *J. Am. Chem. Soc.* **1989**, *109*, 7025.
(8) Stein, C. A.; Taube, H. *J. Am. Chem. Soc.* **1981**, *103*, 693.
(9) Stein, C. A.; Lewis, N. A.; Seitz, G. *J. Am. Chem. Soc.* **1982**, *104*, 2596.
(10) Lewis, N. A.; Obeng, Y. S. *J. Am. Chem. Soc.* **1988**, *110*, 2306.
(11) Lewis, N. A.; Obeng, Y. S.; Taveras, D. V.; van Eldik, R. *J. Am. Chem. Soc.* **1989**, *111*, 924.

0002-7863/92/1514-4345$03.00/0

Table I. Crystallographic Data for 1

formula	$RuSP_2F_{12}N_5C_3H_{23}$
fw	552.31
a, Å	8.3664 (5)
b, Å	12.337 (1)
c, Å	17.780 (1)
β, deg	100.388 (5)
V, Å^3	1805.1 (4)
Z	4
space group	$P2_1/n$
λ, Å	0.71073
D_{calcd} (D_{measd}), g cm^{-3}	2.032 (2.02 (1))
linear abs coeff, cm^{-1}	12.5
2θ range, deg	4–54
temp, K	296 (1)
no. unique data collected	3845
no. data in refinement	3475 ($F_o^2 > 3\sigma(F_o^2)$)
no. of parameters	325
final R_F (R_{wF})	0.042 (0.072)

mophores exhibit a Ru(II) → Ru(III) metal-to-metal charge-transfer (intervalence) absorption band in the near-IR region whose energy depends in part upon the reorganizations that the metal ion coordination sphere, ligand, and solvent shells undergo as part of the intervalence electron transfer process. To help understand the electronic and structural differences between Ru(II)- and Ru(III)-thioether bonding, we present here detailed structural, spectroscopic, and computational studies of $(NH_3)_5Ru^{II}$-thioether systems. Particular attention is focused on the structural and computational results pertinent to a rationalization of Ru(II) → thioether back bonding. Comparisons are drawn to our previous studies of the Ru(III)-thioether analogues.[13]

Experimental and Computational Section

1. Preparation of $Ru^{II}(NH_3)_5S(CH_3)(C_2H_5)\cdot 2PF_6$, 1. Complex **1** was prepared by following a published method[1] using some modifications to obtain single crystals. In a typical preparation, 25.0 mg (0.085 mmol) of $[Ru(NH_3)_5Cl]Cl_2$ was added to a solution of 20.0 mg (0.086 mmol) of Ag_2O in 0.3 mL of 2 M trifluoroacetic acid. The solution was filtered, diluted to approximately 7 mL with water (pH = 2.0), reduced with zinc amalgam for 30 min, and then transferred by cannula to a flask that contained 0.05 g (0.31 mmol) of NH_4PF_6 under argon. The solution was filtered under argon and layered with 1.0 mL of methyl ethyl sulfide. Pale yellow crystals suitable for X-ray diffraction formed over several days at the interface of the layered solution. The size and quality of the crystals was found to depend on the amount of NH_4PF_6.

2. Spectroscopic Measurements. Electronic spectral measurements were made using a computer-interfaced spectrometer built by Aviv Associates that utilizes a Cary Model 14 monochromator and cell compartment. Low-temperature spectra (80 K) were measured in CH_3OH glasses using an Air Products optical Dewar. The glasses were formed between circular quartz windows separated by rubber spacers.

3. X-ray Diffraction Studies. A crystal of **1** approximately 0.35 × 0.35 × 0.58 mm was mounted in a capillary tube under argon. Diffraction measurements were made using an Enraf-Nonius CAD-4 diffractometer and Mo Kα radiation. The Enraf-Nonius Structure Determination Package[14] was used for data collection, data processing, and structure solution. Crystal data and additional details of the data collection and refinement are presented in Table I. Intensity data were collected and corrected for decay, absorption (empirical, ψ-scan), and Lp effects.

The structure was solved by direct methods[15] and refined on F by using full-matrix least-squares techniques. An E map based on 271 phases from the starting set with the highest combined figure of merit revealed coordinates for the Ru and S atoms. The remaining non-H atoms were located from successive difference Fourier maps. Both PF_6 groups were found to be substantially disordered and were difficult to model. On the basis of peak heights from difference electron density maps, each was modeled with P atoms on fully occupied sites and two sets of F atoms with occupancies of 0.6 and 0.4; all atoms of the PF_6 groups were refined anisotropically. Other models, including one with ordered PF_6 groups and one in which the F atoms on partially occupied sites were refined isotropically, led to substantially poorer agreement. Following refinement of the non-H atoms, several H atoms were located from a difference map. Coordinates for the remaining H atoms were calculated by assuming idealized bond geometries and C–H and N–H distances of 0.95 and 0.87 Å, respectively. H atom temperature factors were set according to $B_H = 1.3B_N$, where N is the atom bonded to H. H atom parameters were not refined. Refinement with all non-H atoms anisotropic led to convergence with $R_F = 0.042$, $R_{wF} = 0.072$, and GOF = 2.82. Several large correlation coefficients were observed among the F atom parameters, the largest of which was 0.84. The highest two peaks on the final difference map (1.14, 0.94 e/Å^3), and the only two larger than the largest negative peak (−0.84 e/Å^3) were located 0.46 and 0.41 Å, respectively, from atom F(1). The largest cation residual was 0.45 e/Å^3.

Table II. Fractional Atomic Coordinates and Equivalent Isotropic Thermal Parameters for 1[a]

	x	y	z	B_{eq} (Å^2)
Ru	0.08440 (3)	0.27185 (3)	0.89769 (2)	1.995 (6)
S	−0.0300 (1)	0.30249 (8)	1.00510 (6)	2.45 (2)
P(1)	0.9508 (1)	0.0287 (1)	0.65543 (7)	3.05 (2)
P(2)	0.5414 (1)	0.9916 (1)	0.86047 (7)	3.11 (2)
F(1)[b]	0.9141 (7)	0.1539 (3)	0.6533 (3)	5.4 (1)
F(2)	1.004 (1)	0.0398 (7)	0.7429 (4)	11.8 (3)
F(3)	0.9740 (7)	−0.0992 (4)	0.6582 (3)	4.9 (1)
F(4)	1.128 (1)	0.065 (1)	0.6514 (7)	16.8 (4)
F(5)	0.7750 (7)	0.0025 (7)	0.6392 (6)	12.4 (3)
F(6)	0.967 (1)	0.0217 (8)	0.5685 (4)	11.5 (3)
F(7)	0.504 (1)	1.0983 (9)	0.9010 (7)	15.4 (4)
F(8)	0.7194 (7)	1.0208 (6)	0.8979 (5)	9.4 (2)
F(9)	0.6046 (9)	0.9123 (7)	0.8050 (4)	10.0 (2)
F(10)	0.3747 (9)	0.9745 (8)	0.8119 (5)	12.5 (3)
F(11)	0.550 (1)	0.9031 (6)	0.9215 (4)	9.8 (2)
F(12)	0.574 (1)	0.091 (1)	0.8120 (7)	15.4 (4)
F(1A)	0.889 (1)	0.031 (1)	0.7295 (5)	11.2 (3)
F(1B)	0.817 (1)	−0.009 (2)	0.6952 (8)	16.7 (5)
F(1C)	1.126 (1)	0.0350 (9)	0.7075 (5)	8.4 (2)
F(1D)	1.061 (1)	0.039 (1)	0.5953 (5)	7.4 (3)
F(1E)	1.019 (2)	−0.099 (1)	0.6598 (9)	11.7 (2)
F(1F)	0.813 (1)	0.0198 (8)	0.5814 (5)	7.2 (2)
F(2A)	0.700 (1)	0.043 (1)	0.8563 (7)	9.3 (3)
F(2B)	0.372 (1)	0.939 (1)	0.8607 (8)	12.6 (4)
F(2C)	0.4688 (7)	1.0774 (6)	0.9100 (4)	4.8 (1)
F(2D)	0.499 (1)	1.0611 (9)	0.7851 (5)	8.6 (3)
F(2E)	0.595 (1)	0.8903 (7)	0.8212 (7)	8.5 (3)
F(2F)	0.356 (1)	0.041 (2)	0.0637 (7)	13.0 (5)
N(1)	0.0793 (4)	0.4436 (3)	0.8829 (2)	3.52 (8)
N(2)	0.3253 (5)	0.2828 (3)	0.9649 (2)	3.27 (8)
N(3)	0.0928 (4)	0.0991 (3)	0.9085 (2)	3.46 (8)
N(4)	−0.1458 (5)	0.2584 (4)	0.8199 (2)	3.45 (8)
N(5)	0.2004 (5)	0.2587 (3)	0.7984 (2)	3.11 (7)
C(1)	0.0471 (7)	0.2120 (5)	1.0822 (3)	4.3 (1)
C(2)	−0.2421 (6)	0.2683 (5)	0.9917 (3)	4.4 (1)
C(3)	−0.0153 (9)	0.2332 (6)	1.1561 (4)	5.9 (2)

[a] The equivalent isotropic displacement parameter B_{eq} is defined as $(^4/_3)[a^2B_{11} + b^2B_{22} + c^2B_{33} + ab(\cos\gamma)B_{12} + ac(\cos\beta)B_{13} + bc\cdot(\cos\alpha)B_{23}]$. [b] Atom multipliers for atoms F(1) through F(12) were 0.6; for atoms F(1A) through F(2F), atom multipliers were 0.4.

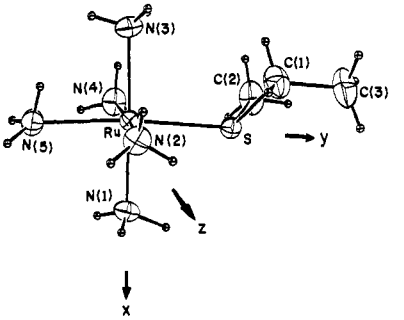

Figure 1. View of the cation in **1** showing the atom numbering scheme.

(12) Lewis, N. A.; Obeng, Y. S. *J. Am. Chem. Soc.* **1989**, *111*, 7624.
(13) Krogh-Jespersen, K.; Zhang, X.; Westbrook, J. D.; Fikar, R.; Nayak, K.; Kwik, W.-L.; Potenza, J. A.; Schugar, H. J. *J. Am. Chem. Soc.* **1989**, *111*, 4082.
(14) Enraf-Nonius Structure Determination Package, Enraf-Nonius, Delft: Holland, 1983.
(15) Main, P.; Fiske, S. J.; Hull, S. E.; Lessinger, L.; Germain, G.; Declercq, J.-P.; Woolfson, M. M. MULTAN 82. A System of Computer Programs for the Automatic Solution of Crystal Structures from X-ray Diffraction Data; University of York, England and Louvain, Belgium, 1982.

Table III. Bond Distances (Å) and Angles (deg) for the Cation in **1**

Ru–S	2.316 (1)	Ru–N(5)	2.168 (4)
Ru–N(1)	2.135 (4)	S–C(1)	1.795 (6)
Ru–N(2)	2.154 (4)	S–C(2)	1.797 (6)
Ru–N(3)	2.139 (5)	C(1)–C(3)	1.521 (9)
Ru–N(4)	2.165 (4)		
S–Ru–N(1)	86.4 (1)	N(2)–Ru–N(4)	174.0 (2)
S–Ru–N(2)	91.0 (1)	N(2)–Ru–N(5)	86.8 (2)
S–Ru–N(3)	95.7 (1)	N(3)–Ru–N(4)	89.5 (2)
S–Ru–N(4)	95.0 (1)	N(3)–Ru–N(5)	89.2 (2)
S–Ru–N(5)	174.6 (1)	N(4)–Ru–N(5)	87.2 (2)
N(1)–Ru–N(2)	90.1 (2)	Ru–S–C(1)	112.5 (2)
N(1)–Ru–N(3)	177.8 (2)	Ru–S–C(2)	113.4 (2)
N(1)–Ru–N(4)	90.1 (2)	C(1)–S–C(2)	99.5 (3)
N(1)–Ru–N(5)	88.6 (2)	S–C(1)–C(3)	114.9 (4)
N(2)–Ru–N(3)	90.0 (2)		

Final atomic parameters are listed in Table II, while a view of the cation, showing the atom numbering scheme and the coordinate axes used for the MO calculations, is given in Figure 1. Selected bond distances and angles for **1** are listed in Table III. Lists of anisotropic thermal parameters, bond distances and angles involving the disordered PF_6 groups, H atom parameters, and observed and calculated structure factors are available.[16]

4. Computational Details. Ab initio MO calculations were performed on the electronic ground state of $(NH_3)_5Ru^{II}S(CH_3)_2$ using the GAUSSIAN 90 series of electronic structure programs[17] and a locally modified version of the GAMESS program package.[18] Wave functions for the closed shell singlet ground state were generated with the restricted Hartree–Fock (HF) method of Roothaan,[19a] and electron correlation effects were investigated at the Moller–Plesset level of perturbation theory carried through second (MP2) or third (MP3) order.[19b] Electronic population indices were derived with the natural atomic orbital (NAO) procedures proposed by Weinhold et al.[19c] Amplitude contour plots of selected MOs were drawn using locally developed graphics routines.

As in our previous work,[7,13] the inner electrons on Ru ($KLM4s^24p^6$), S (KL), N (K), and C (K) have been replaced by ab initio effective core potentials (ECPs). For Ru and S we used the relativistic ECPs developed by Christiansen and Ermler,[20a,b] whereas for N and C we used the non-relativistic ECPs developed by Stevens, Basch, and Krauss.[20c] Minimal valence basis sets were always used for both the H 1s orbital (STO-3G)[20d] and the N 2s and 2p orbitals ((4s, 4p) → [4/4]).[20c] Two basis sets were used for the Ru, S, and C atoms. Molecular basis set I (BSI) consisted of a Ru (3s, 3p, 4d) valence basis contracted [2, 1/2, 1/3, 1];[20a] a S (4s, 4p) valence basis set[20b] augmented with a set of cartesian d-functions[20e] and contracted [3, 1/3, 1/1]; a C (4s, 4p) valence basis set contracted [3, 1/3, 1];[20c] and the above mentioned basis functions on N and H. BSI contains 91 basis functions covering 33 electron pairs and is of valence double-ζ (Ru, C) or slightly better (S) quality for the main atoms of interest. We constructed a more diffuse basis set (BSII) by augmenting BSI with a third set of cartesian d-functions on Ru (exponent = 0.07025) and leaving all the s functions uncontracted ((3s, 3p, 5d) → [1, 1, 1/2, 1/3, 1, 1]); by adding a diffuse sp set[20f] and a second set of d-functions (exponent = 0.15) to the S basis set ((5s, 5p, 2d) → [3, 1, 1/3, 1, 1/1, 1]); and by adding a set of diffuse sp functions on C ((5s, 5p) → [3, 1, 1/3, 1, 1]).[20f] BSII contains 116 basis functions and approaches triple-ζ valence plus polarization quality for Ru, S, and C.

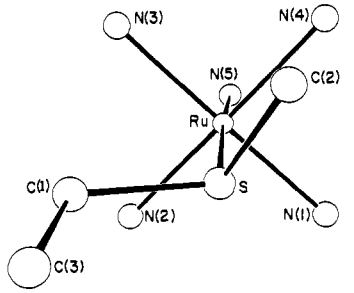

Figure 2. View of the cation in **1** showing the relative orientation of the thioether and $(NH_3)_5Ru$ groups.

Electronically excited states of the $(NH_3)_5Ru^{II}S(CH_3)_2$ complex were investigated using the semiempirical all-valence electron INDO/S MO method as implemented in the ESPPAC program.[21,22] Atomic parameters for Ru, S, N, C, and H were the same as those employed previously in our studies of Ru(III)–imidazole and Ru(III)–thioether complexes.[7,13] Calculations were made with and without the inclusion of d-orbitals on S.[21c] The experimental X-ray structure determined in this work was used as the reference geometry with the ethyl group replaced by a methyl group. The structure was regularized to C_s symmetry and standard bond lengths and angles applied for the H atoms.[23] Excited states were calculated in the singly excited configuration interaction (SECI) and in the time-dependent Hartree–Fock (TDHF) approximations with an excitation space consisting of all possible elementary excitations (~1100).[24,25] Oscillator strengths were computed in the dipole-length approximation with atomic sp and pd terms included. Electronic population analyses on the HF and SECI wave functions were based on one-electron reduced density matrices computed in the zero-differential-overlap (ZDO) approximation.

Results and Discussion

Crystal Structure. The structure of **1** contains $A_5Ru^{II}L$ cations [A = NH_3, L = methyl ethyl thioether] separated by disordered hexafluorophosphate anions. Five $N(NH_3)$ atoms and the thioether S atom complete a distorted octahedron about Ru; bond angles with Ru as vertex (Table III) are all within 6° of the values for a perfect octahedron. The Ru–N distances span a relatively narrow range (2.135 (4) to 2.168 (4) Å) and are comparable to those observed for other $A_5Ru^{II}L'$ and $(A_5Ru^{II})_2L'$ cations (2.122 (7) to 2.203 (8) Å).[26-29] As expected from simple electrostatic considerations, the Ru(II)–N distances are longer than corresponding Ru(III)–N distances in A_5RuS(thioether) complexes (Table IV).[13]

Ru(II)–S bond distances have been reported[30] to span a wide range from 2.188 (3) Å in $(NH_3)_5Ru^{II}DMSO$[29] to 2.450 (3) Å for one of the *cis*-thiobenzoato ligands in $Ru^{II}(phen)(PMe_2Ph)_2(PhC(O)S)_2$.[31] This variation in distance has been attributed in part to varying amounts of π back bonding arising from overlap of filled Ru d(π) orbitals with vacant antibonding orbitals of π-acceptor ligands such as thioethers or DMSO. The Ru(II)–S bond distance is 2.316 (1) Å in the present structure, near the middle of the range. In contrast to the Ru–N distances,

(16) Supplementary material.

(17) Frisch, M. J.; Head-Gordon, M.; Trucks, G. W.; Foresman, J. B.; Schlegel, H. B.; Raghavachari, K.; Robb, M.; Binkley, J. S.; Gonzalez, C.; Defrees, D. J.; Fox, D. J.; Whiteside, R. A.; Seeger, R.; Melius, C. F.; Baker, J.; Martin, R. L.; Kahn, L. R.; Stewart, J. J. P.; Topiol, S.; Pople, J. A. GAUSSIAN 90; Gaussian, Inc.: Pittsburgh, PA, 1990.

(18) Schmidt, M. W.; Boatz, J. A.; Baldridge, K. K.; Koseki, S.; Gordon, M. S.; Elbert, S. T.; Lam, B. QCPE Bulletin, **1987**, *7*, 115. Westbrook, J. D.; Blair, J. T.; Krogh-Jespersen, K. unpublished.

(19) (a) Roothaan, C. C. J. *Rev. Mod. Phys.* **1951**, *23*, 69. (b) Pople, J. A.; Seeger, R.; Krishnan, R. *Int. J. Quant. Chem. Symp.* **1977**, *11*, 149. Moller, C.; Plesset, M. S. *Phys. Rev.* **1934**, *46*, 618. (c) Reed, A. E.; Weinhold, F. *J. Chem. Phys.* **1983**, *78*, 4066. Reed, A. E.; Weinstock, R. B.; Weinhold, F. *J. Chem. Phys.* **1985**, *83*, 735.

(20) (a) LaJohn, L. A.; Christiansen, P. A.; Ross, R. B.; Atashroo, T.; Ermler, W. C. *J. Chem. Phys.* **1987**, *87*, 2812. (b) Pacios, L. F.; Christiansen, P. A. *J. Chem. Phys.* **1985**, *82*, 2664. (c) Stevens, W. J.; Basch, H.; Krauss, M. *J. Chem. Phys.* **1984**, *81*, 6026. (d) Hehre, W. J.; Stewart, R. F.; Pople, J. A. *J. Chem. Phys.* **1969**, *51*, 2657. (e) Francl, M. M.; Pietro, W. J.; Hehre, W. J.; Binkley, J. S.; Gordon, M. S.; Defrees, D. J.; Pople, J. A. *J. Chem. Phys.* **1982**, *77*, 3654. (f) Clark, T.; Chandrasekhar, J.; Spitznagel, G. W.; Schleyer, P. v. R. *J. Compul. Chem.* **1983**, *4*, 294.

(21) (a) Ridley, J.; Zerner, M. *Theor. Chim. Acta.* **1973**, *32*, 111. (b) Zerner, M. C.; Loew, G. H.; Kirchner, R. F.; Mueller-Westerhoff, U. T. *J. Am. Chem. Soc.* **1980**, *102*, 589. (c) Parameters for the S(d) orbitals were taken from the ZINDO program: Zerner, M. C. University of Florida, Gainesville, FL, 1985.

(22) Westbrook, J. D.; Krogh-Jespersen, K. ESPPAC, a semiempirical electronic structure program for the computation of excited state properties; Rutgers University, New Brunswick, NJ, 1989.

(23) Pople, J. A.; Gordon, M. *J. Am. Chem. Soc.* **1967**, *89*, 4253.

(24) Linderberg, J.; Ohrn, Y. *Propagators in Quantum Chemistry*; Academic Press: New York, 1973.

(25) Krogh-Jespersen, K.; Ratner, M. A. *Theor. Chim. Acta* **1978**, *47*, 283.

(26) Lehmann, H.; Schenk, K. J.; Chapuis, G.; Ludi, A. *J. Am. Chem. Soc.* **1979**, *101*, 6197.

(27) Furholz, U.; Joss, S.; Burgi, H. B.; Ludi, A. *Inorg. Chem.* **1985**, *24*, 943.

(28) Henderson, W. W.; Bancroft, B. T.; Shepherd, R. E.; Fackler, J. P., Jr. *Organometallics* **1986**, *5*, 506.

(29) March, F. C.; Ferguson, G. *Can. J. Chem.* **1971**, *49*, 3590.

(30) James, B. R.; Pacheco, A.; Rettig, S. J.; Ibers, J. A. *Inorg. Chem.* **1988**, *27*, 2414.

(31) Gould, R. O.; Stephenson, T. A.; Thomson, M. A. *J. Chem. Soc., Dalton Trans.* **1980**, 804.

Table IV. Comparison of $(NH_3)_5Ru^{II,III}S$(thioether) Structural Parameters

	$A_5Ru^{II}S(CH_3)(C_2H_5)$[a] 1	$A_5Ru^{III}S(CH_3)(C_2H_5)$[b] 2	$A_5Ru^{III}THT$[b,c] 3
Ru-S, Å	2.316 (1)	2.3711 (5)	2.3666 (7)
Ru-N(trans), Å	2.168 (4)	2.126 (2)	2.109 (2)
Ru-N(cis, av) Å	2.148 (14)	2.105 (5)	2.111 (3)
S-C, Å	1.795 (6)	1.822 (2)	1.827 (3)
	1.797 (6)	1.805 (2)	1.816 (3)
S-Ru-N(trans), deg	174.61 (1)	176.08 (5)	176.41 (6)
C-S-C, deg	99.5 (3)	100.7 (1)	94.2 (2)
Ru-S-X,[d] deg	127.2	122.1	125.5

[a] This work. [b] Data from ref 13. [c] THT = tetrahydrothiophene. [d] X is a point on the CSC bisector; see text.

Table V. Calculated and Experimental Geometries of $S(CH_3)_2$, A_5RuL^{2+}, and A_5RuL^{3+} (A = NH_3, L = $S(CH_3)_2$) Complexes[a]

	HF/BSI		HF/BSII		exp[b]		HF/BSII (exp)[c]
	A_5RuL^{2+}	L	A_5RuL^{2+}	L	A_5RuL^{2+}	L	A_5RuL^{3+}
S-C	1.825	1.808	1.833	1.813	1.796	1.805	1.850 (1.825)
C-S-C	104.0	100.4	103.2	100.2	99.5	99.1	104.5 (100.7)
Ru-S	2.532		2.487		2.316		2.419 (2.374)
Ru-N(1)	2.153		2.144		2.135		2.107 (2.110)
Ru-N(2)	2.156		2.148		2.154		2.124 (2.110)
Ru-N(3)	2.153		2.146		2.139		2.103 (2.105)
Ru-N(4)	2.156		2.148		2.165		2.124 (2.110)
Ru-N(5)	2.144		2.135		2.168		2.118 (2.112)
S-Ru-N(3)	93.9		92.7		95.7		92.8 (92.0)
S-Ru-N(5)	177.1		177.6		174.6		179.2 (176.3)
S-Ru-N(1)	85.2		86.3		86.4		87.2 (88.1)
Ru-S-X[d]	135.8		131.7		127.2		137.1 (123.8)[e]

	MP2/BSI		MP2/BSII	MP3/BSI	MP3/BSII
	A_5RuL^{2+}	L	A_5RuL^{2+}	A_5RuL^{2+}	A_5RuL^{2+}
S-C	1.843	1.826			
C-S-C	101.9	99.5			
Ru-S	2.368		2.259	2.399	2.296
Ru-S-X	135.1				

[a] Bond lengths in Å, angles in deg. [b] X-ray data for complex from present work. Electron diffraction structure for L from ref 34. [c] Averaged experimental X-ray structure from our previous work, ref 13, Table VI. [d] X is a point on the CSC bisector; see text. [e] The estimated value for this angle is 133.3° for L = $S(CH_3)_2$, only 6° less than the calculated value.[13]

which are longer for the Ru(II) species, the Ru(II)-S distance is 0.055 Å shorter than that in the corresponding Ru(III) analogue **2** (Table IV), implying substantial back bonding. The Ru(II)-S distance is also substantially smaller than the values reported for the Ru(II)-S(thioether) linkages in the related octahedral Ru(II) complexes *mer-trans*-$Ru(NO)Br_3(n\text{-}Pr_2S)_2$ [2.414 (2), 2.417 (2) Å],[32] *mer*-$Ru(NO)Br_3(Et_2S)(Et_2SO)$ [2.412 (4) Å],[32] and Br_2-(DMSO)(3-ethylthio)-1-(((3-(ethylthio)propyl)sulfinyl)-propane)ruthenium(II) [2.372 (2), 2.393 (2) Å].[33]

The methyl ethyl thioether ligand in **1** is bonded to Ru with pyramidal coordination about S, as has been observed for other Ru-thioether complexes.[13,30] Its orientation with respect to the $(NH_3)_5Ru$ group (Figure 2) is strikingly similar to that observed for **2**, the Ru(III) analogue of **1**. Thus, the S atom lies below the plane defined by Ru, N(2), N(4), and N(5), while the C atoms bonded to S lie above this plane and the C(1)-S-C(2) plane is tilted with respect to the plane of the ammines cis to S [N(1)-N(4)]. The Ru-S-X angle, 127.2°, where X is the midpoint of the C(1)···C(2) vector (Figure 1), gives an estimate of this tilt. As measured by this angle, the tilt in the Ru(II) structure **1** is slightly larger than that in the Ru(III) analogue **2** (Table IV), possibly owing to the shorter Ru-S distance in **1**.

Both the S-C distances and the C-S-C angles are close to those reported for free $S(CH_3)_2$ [1.807 (2) Å, 99.05 (4)°][34] and for the cation in **2** [1.822 (2), 1.805 (2) Å, 100.7 (1)°],[13] which differs from the cation in the present structure only by a change in oxidation state. In the ruthenium nitrosyl complexes noted above, the corresponding distances and angles lie in the ranges 1.803 (12)-1.93 (2) Å and 99.3 (9) - 100.8 (5)°, respectively.

Computed Ground State Geometry. Optimized geometries of dimethyl thioether and the $A_5Ru^{II}S(CH_3)_2$ complex from the ab initio MO calculations are listed in Table V along with pertinent experimental data. For comparison, we also show the geometry of the $A_5Ru^{III}S(CH_3)_2$ complex optimized with BSII as well as averaged X-ray data for $A_5Ru^{III}L$ (L = dimethyl thioether, methyl ethyl thioether, and tetrahydrothiophene) species.[13,35] The coordinate system (Figure 1) used in this discussion is chosen so that the symmetry plane (*xy*) bisects the C-S-C angle and contains the N(1), N(3), N(5), Ru, and S atoms with the coordinate axes essentially directed along N(3)-Ru-N(1) (*x*), N(5)-Ru-S (*y*), and N(4)-Ru-N(2) (*z*). The computed gross geometry of the present Ru(II)-thioether complex is similar to that of the Ru(III)-thioether complex studied previously[13] with the coordination sphere around either Ru atom showing significant distortion from octahedral geometry only in the direction of the thioether ligand. We will focus on the local Ru-S geometry and bonding below and note here only that all N-Ru-N bond angles are within a few degrees of the values appropriate for a perfect octahedron; that the five Ru-N bond lengths span a narrow range (2.135-2.148 Å, HF/BSII), very close to the experimental value in $Ru(NH_3)_6^{2+}$ (Ru-N = 2.144 Å)[36] and that the computed geometrical features associated with the Ru-N ligation match the crystallographic determinations in **1** very well. The computed geometry of the free thioether ligand is also in excellent agreement with the experimental structure obtained by electron diffraction.[34]

The calculations produce a properly oriented thioether ligand as measured by the tilt angle (Ru-S-X ~ 130-135°), but the

(32) Coll, R. K.; Fergusson, J. E.; McKee, V.; Page, C. T.; Robinson, W. T.; Keong, T. S. *Inorg. Chem.* **1987**, *26*, 106.
(33) Riley, D. P.; Oliver, J. D. *Inorg. Chem.* **1986**, *25*, 1821.
(34) Iijima, T.; Tsuchiya, S.; Kimura, M. *Bull. Chem. Soc. Jpn.* **1977**, *50*, 2564.
(35) The present computed structure for $(NH_3)_5Ru^{III}S(CH_3)_2$ differs insignificantly from that obtained previously in ref 13 with a somewhat different but smaller basis set.
(36) Stynes, H. C.; Ibers, J. A. *Inorg. Chem.* **1971**, *10*, 2304.

Ru(II)–S bond length is computed far too long. At the HF/BSI level, the discrepancy between the computed (2.53 Å) and experimental (2.32 Å) values exceeds 0.2 Å (Table V), and reoptimization with BSII only shortens the Ru(II)–S bond by 0.04 to 2.49 Å. This result was surprising as well as disturbing since similar ab initio MO techniques performed well in determining the equilibrium structure of the analogous $A_5Ru^{III}S(CH_3)_2$ complex;[13] for example, the HF/BSII optimized Ru(III)–S bond length is 2.419 Å (Table V), only about 0.04 Å longer than the experimental value. We thus compute, incorrectly, at this level, that the Ru(III)–S bond length should be considerably shorter (~0.1 Å) than the Ru(II)–S bond length.

We carried out geometry optimizations with several other effective core potentials and basis sets,[37] and even an all-electron representation of the thioether ligand and a less restrictive core potential on Ru (covering only the KLM shells) were tried. Quantitatively similar results (Ru(II)–S > 2.5 Å) were always obtained. Also, it was determined that f-type basis functions on Ru (in conjunction with BSI) did not play a significant role in determining the Ru–S distance; in fact, the Ru(II)–S bond length of 2.487 Å (HF/BSII, Table V) is the shortest we encountered throughout this extensive series of calculations. We conclude that it is necessary to go beyond the HF approximation to describe the Ru(II)–thioether electronic interactions properly.

Electron correlation effects were investigated by selective optimizations of key structural variables using Moller–Plesset perturbation theory through second (MP2) or third order (MP3).[19b] A series of exploratory calculations using MP2 theory in conjunction with BSI showed that the internal geometrical structure of free or complexed $S(CH_3)_2$ was not very sensitive to inclusion of correlation contributions (S–C bond lengths increase by about 0.02 Å, C–S–C angle closes by 1–2°; cf. the HF/BSI and MP2/BSI results in Table V). The Ru–S–X tilt angle was also rather insensitive to correlation effects (Table V). However, the Ru–S bond length decreased considerably (by 0.16 Å) from 2.53 (HF/BSI) to 2.37 Å (MP2/BSI). There are, however, well documented cases where the application of MP2 theory overestimates the structural changes relative to HF theory[38] and, indeed, upon reoptimization at the MP3 level the Ru–S bond lengthened by 0.03 Å to a value of 2.40 Å (MP3/BSI, Table V), nearly 0.1 Å longer than the experimental value. On the basis of these results, only the Ru–S distance was varied in a final series of correlated calculations using the larger basis set (BSII). Starting from the HF/BSII structure (Ru–S = 2.487 Å), we obtained a decrease in the Ru–S bond length at the MP2 level of nearly 0.25 Å to 2.259 Å (MP2/BSII), a value now smaller than the experimental distance. Again, application of higher order theory generated a small increase (~0.04 Å) in the bond length. Our best computed value for the Ru–S bond length, obtained at the level of third order Moller–Plesset perturbation theory with a basis set of near triple-ζ valence plus polarization quality on the important atoms, is 2.296 Å (MP3/BSII) and is within 0.020 Å of the experimental value (2.316 (1) Å, Table V).

Both Ru(II)– and Ru(III)–S(thioether) interactions are inherently weak, and the potential energy surfaces are flat as functions of the Ru–S distance or the Ru–S–X tilt angle.[13] For example, the energy increases by only 0.7 kcal/mol (250 cm^{-1}) upon a 0.05 Å increase in the Ru(II)–S distance beyond the minimum. Even larger basis sets or inclusion of additional electron correlation, e.g., through higher order perturbation theory (MP4), would presumably alter the position of the structural minimum although changes from, say, the MP3 to the MP4 level would be expected to be even smaller than those computed from MP2 vs MP3 theory (~0.035 Å). We thus conclude not only that electron correlation is important in the computational description of the Ru(II)–S interactions but also that the near perfect agreement between computed and experimental Ru–S bond lengths, and hence overall complex geometry, ultimately obtained in this work should be considered slightly fortuitous. Exploratory calculations on the oxidized $A_5Ru^{III}S(CH_3)_2$ species indicate that electron correlation contributions also shorten the Ru^{III}–S bond, although to a comparatively smaller extent than the reductions computed for the Ru(II)–S bond lengths.[39]

Ground State Electronic Structure. The electronic structure of $S(CH_3)_2$ has been discussed previously.[13] Only the highest occupied MO, an out-of-plane lone pair concentrated (>90%) on the S atom, S(π), can serve as a good electron donor. The next two occupied orbitals, the symmetric (in-phase) and antisymmetric (out-of-phase) combinations of S–C bond orbitals, lie some 3–4.5 eV lower in energy (both computationally[13] and experimentally (PES)[40,41]) and are spatially and energetically far from optimal for involvement in metal–ligand bonding. The antisymmetric combination has the wrong symmetry to interact with the formally empty Ru d-orbitals and will not be considered further. The second lone pair formally on the divalent S atom is dominantly of 3s character and is positioned much lower in orbital energy than the S–C bond orbitals. Amplitude contour plots of the three upper thioether orbitals are given in ref 13. On the Ru atom, the principal acceptor orbital for thioether electron density is the $d_{x^2-y^2}$ member of the e_g^* set of 4d-orbitals. Maximal S(π)-d(σ^*) electronic interaction would require a fully perpendicular orientation (Ru–S–X = 90°) of the A_5Ru^{2+} and $S(CH_3)_2$ fragments, as in **4**. This orientation is sterically most unfavorable; however, geometry optimization with the Ru–S–X angle fixed at 90° leads to a Ru–S distance larger than 3.1 Å. The Ru–S–X angle must increase to relieve steric crowding. At Ru–S–X = 180°, **5**, steric interactions are minimized but so are the electronic interactions for forward donation from S to Ru, since the S(π) donor orbital and the $d_{x^2-y^2}$ acceptor orbital now are orthogonal. The symmetric

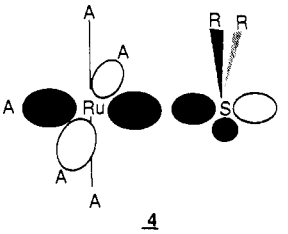

4

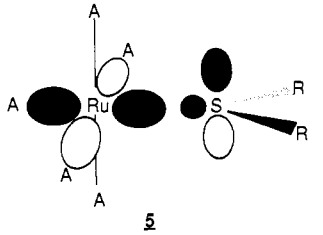

5

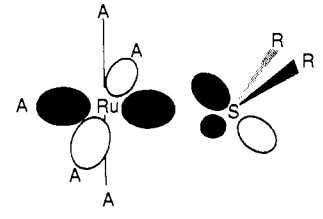

6

S–C bond orbital (S–C(σ)) is not a good electron donor, although it is optimally oriented in **5** to interact with $d_{x^2-y^2}$, and geometry optimization with this ligand orientation also leads to a long Ru–S bond length (>2.6 Å). The Ru–S–X angle must thus take on a value intermediate between 90° and 180° to balance these op-

(37) Hay, P. J.; Wadt, W. R. *J. Chem. Phys.* **1985**, *82*, 270.
(38) (a) Park, C.; Almlof, J. *J. Chem. Phys.* **1991**, *95*, 1629. (b) Nobes, R. H.; Moncrieff, D.; Wong, M. W.; Radom, L.; Gill, P. M. W.; Pople, J. A. *Chem. Phys. Lett.* **1991**, *182*, 216.
(39) Krogh-Jespersen, K.; Ding, Y., unpublished results.
(40) Frost, D. C.; Herring, F. G.; Katrib, A.; McDowell, C. A.; McLean, R. A. N. *J. Phys. Chem.* **1972**, *76*, 1030.
(41) Cradock, S.; Whiteford, R. A. *J. Chem. Soc., Faraday Trans. 2* **1972**, *68*, 281.

posing steric and electronic demands, **6**. The tilt angles in both the Ru(II)–S and Ru(III)–S complexes (Tables IV and V) are similar (122°–137°) and approximately centered between the two possible extremes (**4** and **5**).

The nature of the specific orbitals involved in Ru(II)–S back donation are not intuitively obvious. The d_{xy} metal ion orbital must be the donor in this interaction, but the acceptor could potentially be unoccupied S(d) orbitals, antibonding S–C(σ^*) orbitals, or even the S(π) orbital, acting as both a donor and acceptor orbital in the complex. If S($d_{x^2-y^2}$, d_{xy}) orbitals were predominantly involved, the back donation should be rather insensitive to the value of the Ru–S–X tilt angle; if S–C(σ^*) orbitals were involved, conformations **4** and **5** will, respectively, maximize and minimize the interaction. If no electrons were present in the S(π) orbital, metal–ligand back donation would be maximized in conformation **4** and negligible in **5**. It would seem a priori that metal–ligand back donation could occur effectively into a variety of ligand orbitals at the intermediate tilt angles (**6**) required by the steric considerations and electronic demands for forward donation outlined above.

Amplitude contour plots (Figure 3a,b) of two MOs illustrate considerable mixing between the S(π) orbital and Ru d-orbitals. The HOMO (Figure 3a) is a rehybridized S(π) orbital interacting in an out-of-phase, antibonding manner with metal d-orbitals. It has a computed orbital energy of −16.2 eV (HF/BSII), whereas the in-phase, bonding combination (HOMO-3, Figure 3b) has an orbital energy of −17.9 eV. Both figures show dominance by the Ru(d_{xy}) orbital (i.e., d(π)–p(π) interaction), but the metal orbital contours are actually rotated away from fully bisecting the Ru–ligand bonds, which is graphical evidence that Ru($d_{x^2-y^2}$) orbital character is also present. Two doubly occupied, essentially degenerate Ru d-orbitals (d_{xz}, d_{yz}) are positioned halfway (−17.0 eV, −17.1 eV) between these MOs. The strong mixing of Ru(d_{xy}) and S(π) appears to have its origin in an accidental near degeneracy in orbital energies, since no net stabilization occurs from interaction between two doubly occupied orbitals. The next occupied level is the S–C(σ) orbital (HOMO-4, Figure 3c), which appears to be slightly mixed with a rotated Ru($d_{x^2-y^2}$) orbital. The orbital energy difference between the S–C(σ) (−19.8 eV) and stabilized S(π)(−17.9 eV) orbitals in the complex is 1.9 eV, whereas it is 2.7 eV in the free dimethyl thioether ligand (2.6 eV experimentally from PES),[40,41] indicating a relative stabilization of S(π) in the complex by ~0.8 eV.

Natural atomic orbital (NAO) analyses of the electronic wave functions are helpful in further characterizing the Ru(II)–S interactions.[19c,42] At the HF level at the HF/BSII optimized geometry (Ru–S = 2.487 Å, Table V), the Ru atom carries a positive charge of 0.73e which implies that the formally dipositive ion has received 1.27e from the ligands. Electron donation to the metal is evenly distributed among the six ligands with a net transfer from the entire $S(CH_3)_2$ ligand of 0.18e and an average of 0.22e transferred from each of the NH_3 units.[43] Charge is accepted on Ru almost solely into the $d_{x^2-y^2}$ (0.70e) and d_{z^2} (0.59e) orbitals; only 0.04e and 0.06e are positioned in the 5s and 5p orbitals, respectively. The larger population in the Ru($d_{x^2-y^2}$) acceptor orbital suggests that electron donation by the thioether ligand is stronger than that of an ammine (by ~0.11e). The metal d(π) set has 1.99e in each of the "nonbonding" d_{xz} and d_{yz} orbitals but only 1.89e in the d_{xy} orbital, indicating that back donation (~0.10e) has taken place from this Ru orbital to the thioether. Further analysis shows that the net forward migration of 0.18e from $S(CH_3)_2$ to Ru(II) is contributed solely by the C (0.06e total) and H (0.12e total) atoms; surprisingly, the net charge on the S atom is the same in the complex as in the free ligand. Only the four eclipsing methyl H-atoms positioned out of the CSC plane donate electrons, however, which strongly implies that it is the

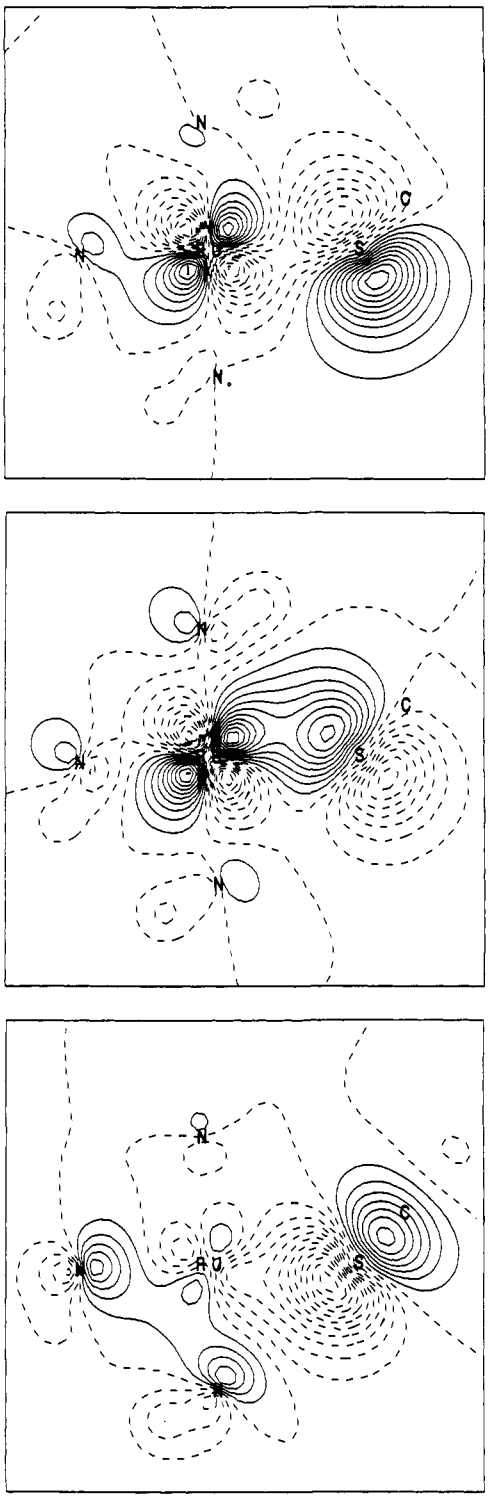

Figure 3. Amplitude contour plots of frontier orbitals in $(NH_3)_5Ru^{II}S(CH_3)_2$. Heavy (dashed) lines indicate positive (negative) amplitude values. All plots are made in the symmetry (xy) plane. (a, top) The HOMO in the complex, an out-of-phase combination of Ru(d_{xy}) and S(π) orbitals. (b, middle) The in-phase combination of the Ru(d_{xy}) and S(π) orbitals mixed with some Ru($d_{x^2-y^2}$) character. (c, bottom) The symmetric combination of S–C(σ) bond orbitals with some admixture of Ru($d_{x^2-y^2}$).

S(π) lone pair orbital, capable of hyperconjugative interaction with π-type CH_3 bond orbitals, that provides the major pathway for electronic interactions with the metal. The total occupancy in the S(d) orbitals is just 0.04e before as well as after ligand complexation, i.e., there are no signs of Ru(II)–S interactions involving S(d)-orbitals. Significant back donation into S–C(σ^*) orbitals should severely alter the internal thioether structure in

(42) The population analyses are relatively insensitive to the actual geometry used.

(43) In the $(NH_3)_5Ru^{III}$–$S(CH_3)_2$ complex where the formal charge on Ru is 1.23e, the donation from each NH_3 unit is slightly larger (0.28e) and the $S(CH_3)_2$ contribution is considerably larger (0.36e), reflecting a stronger electrostatic Ru–S interaction and no Ru(III)–S back donation.

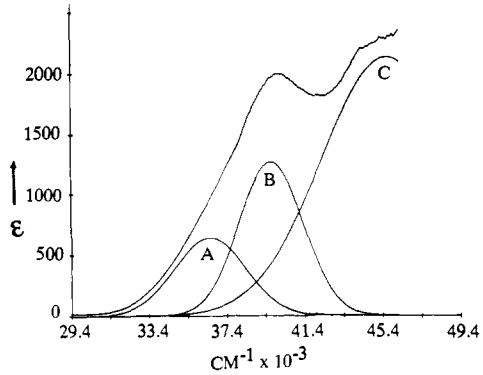

Figure 4. Gaussian deconvoluted UV spectrum of a 2.42×10^{-3} M solution of **1** in methanol at 80 K.

the complex from that of the free ligand, an effect neither observed nor computed. A simplified, pictorial interpretation consistent with the population analysis data is that metal–thioether interactions, including both forward and back donation, involve almost exclusively only the S(π) and the Ru($d_{x^2-y^2}$, d_{xy}) orbitals. The S atom donates about 0.10e to the Ru($d_{x^2-y^2}$) orbital from the S(π) orbital but it also receives an equivalent amount back from the Ru(d_{xy}) orbital into the identical orbital, thus undergoing no net loss of electronic charge. Given the indistinguishable nature of the electrons, however, an equivalent interpretation is that the orientation of the thioether ligand and its principal interacting orbital facilitates direct charge flow (~0.10e) from the Ru(d_{xy}) orbital into the Ru($d_{x^2-y^2}$) orbital.

We find that an additional 0.29e have been allocated to the Ru(II) metal ion by the MP2/BSII wave function relative to the HF/BSII wave function. The thioether ligand is only contributing 0.02e, however, and the remainder (0.27e) comes from the five ammines. More detailed analysis shows that a MP2 correlated wave function increases the net electron density on S in both the free and complexed ligand by about 0.10e, mostly at the expense of the C atoms. This makes the S atom a better electron donor and an additional small amount of electronic charge is forwarded to the Ru(II) metal ion in the complex. The changes in electron populations at the AO level are all very small in absolute terms but the populations in diffuse orbitals increase in general. It is apparently a combination of many small adjustments to the electronic charge distribution that gives rise to the significant reduction in Ru(II)–S distance at the correlated level (Table V).

At our best computed geometry[44] we find that, relative to the values given above, an additional charge of 0.04e has been donated from the thioether to the Ru atom. This transfer occurs exclusively from S(p_x, p_y) orbitals and goes into the Ru($d_{x^2-y^2}$) orbital, consistent with the picture outlined above. The Ru–S bonding interactions occur primarily with S orbitals lying perpendicular to the CSC plane. There are no significant signs of S(d)-orbital involvement or indications of Ru back donation into the S–C(σ^*) orbitals.

Electronic Spectroscopic Results. Electronic solution spectra for a number of A_5Ru^{II} complexes of dimethyl chalcogenides have been reported by Taube and co-workers.[1,45] Absorptions were observed for $A_5Ru^{II}S(CH_3)_2$ at 27 900 cm^{-1} (358 nm, $\epsilon_{max} \sim 64$), 38 750 cm^{-1} (258 nm, $\epsilon_{max} \sim 2150$), and 42 550 cm^{-1} (235 nm, $\epsilon_{max} \sim 2050$). The lowest energy band was assigned as a LF transition and the higher energy bands were tentatively assigned as MLCT. Our room temperature solution spectra of **1** (not shown) agree qualitatively with these data, but the low temperature spectra (80 K, EtOH) reveal additional structure, in particular in the 40 000 cm^{-1} region (Figure 4). Absorption maxima are separated better, and the long absorption shoulder on the low energy side (~36 000 cm^{-1}) of the lower energy band indicates the presence of at least one additional transition in this region.

(44) Our best computed geometry is the basic HF/BSII geometry properly modified with the parameters reoptimized at the MP2 and MP3 levels of theory (Table V).

(45) Stein, C. A.; Taube, H. *Inorg. Chem.* **1979**, *18*, 1168.

Table VI. Atomic Orbital Composition and Orbital Energies of the Frontier Orbitals in $(NH_3)_5Ru^{II}S(CH_3)_2$[a]

orbital[b]	energy[c]	composition[d]
LUMO + 3(a″)	−5.00	0.52S(p_z) − 0.47S(d_{xz}) − 0.41S(d_{yz}) − 0.28C(s)
LUMO + 2(a′)	−5.61	0.60Ru(s) − 0.28S(s) − 0.27S(p_x) + 0.20S(d_{z^2})
LUMO + 1(a′)	−6.16	0.68Ru(d_{z^2}) − 0.28Ru($d_{x^2-y^2}$) − 0.22Ru(d_{xy})
LUMO(a′)	−6.63	0.52Ru($d_{x^2-y^2}$) + 0.32Ru(d_{xy}) + 0.32Ru(d_{z^2}) + 0.26S(p_x)
HOMO(a′)	−15.11	0.74Ru(d_{xy}) − 0.46Ru($d_{x^2-y^2}$) − 0.30S(p_x) + 0.15S(p_y)
HOMO − 1(a″)	−15.26	0.96Ru(d_{xz}) + 0.18Ru(d_{yz})
HOMO − 2(a″)	−15.41	0.94Ru(d_{yz}) − 0.18S(d_{yz}) − 0.17Ru(d_{xz})
HOMO − 3(a′)	−16.96	0.66S(p_x) − 0.40S(p_y) − 0.38Ru($d_{x^2-y^2}$) + 0.21Ru(d_{xy})

[a] Data from INDO/S calculation at the Hartree–Fock level. [b] Mulliken symbols in the C_s point group are in parentheses. [c] Orbital energy in eV. [d] Leading MO coefficients and AO labels; see Figure 1 for the orientation of the coordinate system.

Gaussian deconvolution of the 33 000–47 000-cm^{-1} region is consistent with the presence of two lower energy absorptions at 36 500 cm^{-1} ($\epsilon_{max} \sim 650$) and 39 700 cm^{-1} ($\epsilon_{max} \sim 1300$), and a more intense, higher energy transition peaking at 45 600 cm^{-1} ($\epsilon_{max} \sim 2200$) (Figure 4). The latter transition is not well resolved since it builds upon absorption that steadily increases in intensity toward 50 000 cm^{-1} (200 nm).

The LF spectrum of RuA_6^{2+} is expected to contain two weak absorption features, corresponding to transitions from the ground state of t_{2g}^6 occupancy ($^1A_{1g}$) to excited states of $t_{2g}^5e_g^1$ occupancies ($^1T_{1g}$ and $^1T_{2g}$). Indeed, two clearly resolved maxima have been observed for a number of substituted Ru(II)–hexaammines in the regions 27 000–29 000 cm^{-1} ($\epsilon_{max} \sim 50$, $^1A_{1g} \rightarrow {}^1T_{1g}$) and 33 000–34 000 cm^{-1} ($\epsilon_{max} \sim 100$, $^1A_{1g} \rightarrow {}^1T_{2g}$), respectively.[46-48] The lower energy feature is also readily detected in the parent species at 26 000 cm^{-1} ($\epsilon_{max} \sim 40$),[46-48a] whereas the higher energy feature is not as well resolved (~32 250 cm^{-1}).[48a] As argued convincingly by Schmidtke and Garthoff,[46] a more intense absorption feature near 36 000 cm^{-1} ($\epsilon_{max} \sim 700$) cannot be the "missing" $^1T_{2g}$ absorption component, since this would lead to an imaginary Racah B parameter. Ford et al. have assigned this diffuse band as involving charge transfer to solvent (CTTS) transitions.[48] Absorption in this region might also be associated with the oxidized RuA_6^{3+} complex, which shows a prominent feature near 36 400 cm^{-1} ($\epsilon_{max} \sim 500$).[13,49] Our calculations on the parent RuA_6^{2+} complex predict LF transitions at 25 600 and 31 600 cm^{-1}, respectively, with nearly vanishing oscillator strengths ($f < 10^{-5}$) due to the inherent parity forbiddenness. Absorption maxima for free diethyl thioether in heptane have been reported near 51 200 ($\epsilon_{max} \sim 31\,000$) and 47 000 cm^{-1} ($\epsilon_{max} \sim 16\,000$) with a lower energy, less intense shoulder observed at ~42 000 cm^{-1} ($\epsilon_{max} \sim 600$).[50] On the basis of these comparisons, the LF transitions in **1** may be expected near or below 32 000 cm^{-1}, and some of the absorption at very high energy (>45 000 cm^{-1}) may be solely due to the thioether ligand. However, the two transitions identified between 35 000 and 40 000 cm^{-1}, and perhaps also the higher energy feature at 45 000 cm^{-1}, should be signatures of metal–ligand interactions, although there may be other underlying transitions contributing to the 35 000–40 000-cm^{-1} region (vide supra).

Semiempirical INDO/S calculations for the electronically excited states were carried out on the dimethyl thioether analogue of **1**. The preservation of a symmetry plane facilitates interpretation of the computed data since, with just one exception, only

(46) Schmidtke, H.-H.; Garthoff, D. *Helv. Chim. Acta* **1966**, *49*, 2039.
(47) Endicott, J. F.; Taube, H. *Inorg. Chem.* **1965**, *4*, 437.
(48) (a) Matsubara, T.; Efrima, S.; Metiu, H. I.; Ford, P. C. *J. Chem. Soc., Faraday Trans. 2* **1979**, *75*, 390. (b) Matsubara, T.; Ford, P. C. *Inorg. Chem.* **1978**, *17*, 1747. (c) Hintze, R. E.; Ford, P. C. *J. Am. Chem. Soc.* **1975**, *97*, 2664.
(49) Navon, G.; Sutin, N. *Inorg. Chem.* **1974**, *13*, 2159.

Table VII. Experimental and Calculated Transition Energies (cm^{-1}) and Intensities in **1**[a]

exptl[b]	ϵ_{max}	calcd^{SECI}	f^{SECI}	calcd^{TDHF}	f^{TDHF}	assignment[c]
27 800	100	25 000	0.005	24 800	0.005	$Ru(d_{xy}) \rightarrow Ru(d_{x^2-y^2})$
		31 300	0.003	31 100	0.003	$Ru(d_{xy}) \rightarrow Ru(d_{z^2})$
36 500	650	37 950	0.026	37 750	0.022	$Ru(d_{xy}) \rightarrow S\text{-}C(\sigma^*)$[d]
39 700	1300	39 500	0.087	39 250	0.082	$Ru(d_{xy}) \rightarrow S\text{-}C(\sigma^*)$[e]
45 600	2200	42 700	0.072	42 500	0.072	$S(\pi) \rightarrow Ru(d_{x^2-y^2})$
		45 900	0.026	45 650	0.025	$S(\pi) \rightarrow S(d)$
		47 000	0.130	46 600	0.099	$Ru(d_{xy}) \rightarrow S(d_{xy})$

[a] In the calculations, **1** was modeled by the analogous $A_5Ru^{II}S(CH_3)_2$ complex, see text. [b] At 80 K, see caption of Figure 4. [c] Only the major characteristic of each orbital in the dominant configuration is indicated. [d] Out-of-phase combination of virtual bond orbitals. [e] In-phase combination of virtual bond orbitals.

transitions polarized in this plane are calculated to carry appreciable intensities (oscillator strengths $f > 10^{-3}$) in the spectral region of interest (25 000–50 000 cm^{-1}). The MO ordering near the Fermi level is the same in the semiempirical and ab inito calculations as outlined in Table VI.

In the occupied orbital manifold, the HOMO is the out-of-phase combination of $Ru(d_{xy})$ and $S(\pi)$ orbitals, followed by the remaining two Ru(d) orbitals from the t_{2g} set (HOMO − 1, HOMO − 2), and then the in-phase combination of the $S(\pi)$ and $Ru(d_{xy})$ orbitals (HOMO − 3). An energy gap of more than 2 eV separates HOMO-3 from the S–C σ-orbitals and the core orbitals. Low lying virtual orbitals of spectroscopic relevance include the e_g set of Ru(d) orbitals (LUMO ($d_{x^2-y^2}$), LUMO + 1 (d_{z^2})) and the Ru(5s) orbital mixed with S orbitals (LUMO + 2). The antisymmetric set of S–C(σ^*) bond orbitals is next in the virtual manifold (LUMO + 3) and is followed by a rapid succession of higher lying orbitals, including all the S(3d) orbitals. The major atomic contributors to each MO are used here as illustrative labels only, and the actual MOs do typically contain contributions from many AOs in often nearly equal proportions (Table VI).

The low energy region of the computed spectrum for the $A_5Ru^{II}S(CH_3)_2$ complex is comprised of the LF transitions, calculated at 25 000 (f = 0.005) and 31 300 cm^{-1} (f = 0.003). Individual components are not discernible in the experimental spectrum of **1** and only a broad maximum around 27 800 cm^{-1} ($\epsilon_{max} \sim 100$) is observed. These excited states are configurationally very pure and the HOMO → LUMO and HOMO → LUMO + 1 elementary excitations enter with coefficients larger than 0.9 in the excited state wave functions. The computed spectrum is transparent from ~31 000 to nearly 40 000 cm^{-1} where three transitions are predicted at 37 950 cm^{-1} (f = 0.026), 39 500 cm^{-1} (f = 0.087), and 42 700 cm^{-1} (f = 0.072), respectively. The 37 950 cm^{-1} transition is polarized perpendicular to the molecular plane of symmetry, as the sole exception below 50 000 cm^{-1} alluded to above. It consists of two major components in about equal proportions: (i) the HOMO → LUMO + 3 excitation describing electron transfer from the $Ru(d_{xy})$–$S(\pi)$ orbital to the out-of-phase combination of S–C(σ^*) bond orbitals, and (ii) the HOMO − 3 → LUMO + 3 configuration which is an excitation of more local thioether character. Due to the mixed charge transfer and local excitation character of this transition, the net metal-to-ligand charge transfer is small although substantial charge rearrangements occur at the local AO level. Population analysis of the excited state wave function shows that the Ru atom has lost 0.15e to the thioether ligand, almost exclusively from the d_{xy} orbital. On the thioether ligand, the charge is distributed as an additional 0.10e on S and 0.04e on each C atom. The 39 500 cm^{-1} transition has as its dominant configuration (CI coefficient ~ 0.9) the elementary HOMO → LUMO + 2 excitation, that is, electron transfer from the $Ru(d_{xy})$ to the Ru(5s)+S orbital. In this excited state, the Ru atom donates 0.19e to the thioether ligand, relative to the ground state populations. Both transitions computed below 40 000 cm^{-1} contain MLCT character, and we assign these two transitions to bands A and B in the deconvoluted spectrum of **1** (Figure 4, Table VII).

The transition computed at 42 700 cm^{-1} has the HOMO − 3 → LUMO excitation (CI coefficient ~ 0.7) as its main contributor, i.e., electron promotion from the $S(\pi)$ orbital to the $Ru(d_{x^2-y^2})$ orbital corresponding to LMCT. However, it also contains local thioether excitation character as well as some Ru(d) → S(d) character and the computed net atomic charge transfers are consequently again small. Although the S atom loses 0.52e in this excited state from its 3p orbitals, it receives 0.48e back into the 3d orbitals for an overall net loss of only 0.04e. Similarly, the net gain on the Ru metal is 0.02e although individual orbital populations change much more dramatically. A tentative assignment as LMCT for this transition is thus based more on the nature of the dominant elementary excitation than on the actual amounts of charge moved from the thioether ligand to the Ru metal. We assign this transition to experimental band C (Figure 4, Table VII).

An additional transition is computed nearby at 45 900 cm^{-1} (f = 0.026). This transition is also heavily mixed with component excitations mostly of local thioether ligand character and may be contributing to band system C. We do not think this weak transition appears as a separate feature in **1**, in particular since the next computed transition is only 1100 cm^{-1} higher in energy at 47 000 cm^{-1} and is far more intense (f = 0.130). The two major contributors are HOMO → S(d) and HOMO − 3 → S(d) excitations. In this excited state, the Ru atom is computed to lose 0.12e and the S atom to gain 0.13e; furthermore, the loss from Ru occurs from the d_{xy} orbital, to some extent justifying a Ru(d) → S(d) MLCT label. However, the gross change in atomic charge on S again masks considerable local charge changes at the AO level. The total populations in S(d) orbitals increase by almost 0.70e, primarily from transfer out of the $S(\pi)$ orbital, suggesting an assignment as a local thioether transition. No further intense transitions are computed until beyond 55 000 cm^{-1}, and hence we assign this 47 000 cm^{-1} transition to the sharply rising absorption at the high energy end of the spectrum of **1**. This spectral region is also where the thioether ligand should show moderately strong internal absorption.[50]

The energies of the computed transitions match the observed absorption bands well, typically within ca. 2000 cm^{-1} or so. The relative oscillator strengths are less satisfactory when compared to the experimental ϵ_{max} values. We thus carried out calculations in the time-dependent Hartree–Fock (TDHF) approximation since the inclusion of doubly excited configurations in TDHF generally leads to improved absorption intensities, leaving the transition energies relatively unchanged from SECI.[25,51] The TDHF results are also included in Table VII. Small decreases are computed in the transition energies as expected, and some improvement in relative intensities may also be noted, although the computed intensity ratio for bands B and C (~1:1) remains different from the ratio deduced from the low temperature spectrum (~1:2). The computed intensity ratio matches that of the solution spectrum well, however.[1,45] Overall, no dramatic changes are observed between the results from the SECI and the TDHF calculations.

In summary, we assign bands A and B of Figure 4 as MLCT and band C tentatively as LMCT. From the work of Ford et al.,[48] it appears that these absorptions are built upon rising CTTS absorption whose onset occurs at approximately 33 000 cm^{-1}. The

(50) Spectrum I/7 in *UV-Atlas of Organic Compounds*; Plenum Press: New York, 1968; Vol. IV.

(51) Jorgensen, P.; Simons, J. *Second Quantization-Based Methods in Quantum Chemistry*; Academic Press: New York, 1981. Jorgensen, P. *Ann. Rev. Phys. Chem.* **1975**, *26*, 359.

charge transfer region of the $A_5Ru^{II}S(CH_3)_2$ spectrum occurs at relatively high energy (above 35 000 cm^{-1}) due to the closed shell characteristics of both the metal ion and the ligand. The electron-rich t_{2g}^6 Ru(II) ion is a poor reducing agent[1] and the thioether ligand does not possess any superior acceptor orbitals. The 42 700 cm^{-1} transition assigned to band system C is the only computed transition in which Ru does not act as the electron donor. It is interesting to note that the spectrum of the Ru(II)–thioether complex can actually not be accounted for without the inclusion of S(3d) orbitals. Limiting the S atomic basis set to contain only s and p orbitals leads to a computed spectrum for the $A_5Ru^{II}S(CH_3)_2$ complex that is transparent in the region 31 500 to 53 500 cm^{-1} except for one weak transition at 45 000 cm^{-1}, clearly not in any accordance with experimental observations.[52] The analogous $A_5Ru^{III}S(CH_3)_2$ complex contains only LMCT absorptions,[13] and S(3d) orbitals are of no particular importance for the description of that spectrum. The computed spectrum is moderately dependent on the geometrical orientation of the ligand, and the specific values and assignments given above should be viewed with some caution. Without the guidance of electronic structure calculations, however, detailed assignments for the spectrum of **1**, to which any real measure of confidence can be attached, appear impossible to make.

Concluding Remarks

We have probed the structural, electronic, and spectroscopic features of Ru(II)–thioether bonding in detail. Whereas signs of significant Ru(II)–S back bonding are evident from electrochemical data[1,4] and from the structural and spectroscopic results reported here, clearcut theoretical verification of Ru(II)–S back bonding has proven difficult to obtain. The Hartree–Fock approximation is not fully adequate for the description of the weak, covalent Ru(II)–S interactions, and electron correlation with large, diffuse basis sets must be included in the computational model. Furthermore, the low symmetry of the complex allows many AOs to participate in the Ru(II)–thioether interactions and renders detailed electronic structure analyses difficult. A structurally simpler and stronger π-acceptor such as N_2 diminishes the computational problems. Here the Ru(II)–N_2 bond is computed shorter than the Ru(III)–N_2 bond already at the Hartree–Fock level, and the role of correlation, although still significant, is less than in the Ru(II)/Ru(III)–S case.[53]

Our structural and computational results should be pertinent to calculations of the inner sphere reorganization energies and electronic coupling matrix elements for photoinduced electron transfer between $(NH_3)_5Ru^{II,III}$ units that is mediated by dithiaspiroalkane spacers.[8-12] The reference Ru–S and Ru–N displacements resulting from ground state electron transfer have now been quantified along with the shallowness of the Ru–S potential energy surface, the modest changes in the Ru–S–X tilt angles, and the geometrical parameters of the thioether ligands. The structure of the thioether is invariant to complexation and Ru(II) → Ru(III) oxidation since the major Ru–S bonding interactions involve $Ru(d_{x^2-y^2}, d_{xy})$ and $S(\pi)$ orbitals perpendicular to the SC_2 plane. As noted earlier by Hush and co-workers,[54] coordination about the S donors is expected to be pyramidal. A planar arrangement of the Ru–SC_2 units (Ru–S–X tilt angle = 180°) was assumed by Beratan and Hopfield who estimated the electronic coupling matrix elements for these mixed valence systems using a periodic one-electron potential to describe the through-bond propagation of the Ru wave function tails.[55] Future calculations of the electronic coupling matrix elements can now be based upon the observed molecular and electronic structures of the $(NH_3)_5Ru^{II,III}$–thioether subunits.

Acknowledgment. We thank Professor P. C. Ford for helpful suggestions regarding the spectrum of **1** and reprints. This research was supported by the National Institutes of Health (Grant GM-34111 to K.K.-J. and Grant GM-37994 to H.J.S. and J.A.P.), the National Science Foundation (Grant CHE 89120 to H.J.S. and J.A.P.), the donors of the Petroleum Research Fund, administered by the American Chemical Society (PRF-AC15903 to K.K.-J.), and the David and Johanna Busch Foundation (K.K.-J., H.J.S., and J.A.P.). The diffractometer-crystallographic computing facility was purchased with a grant from the National Institutes of Health (Instrumentation Grant 1510 RRO 1486 O1A1). The computational research was supported by shared equipment grants from the National Science Foundation, the National Institutes of Health, and the New Jersey Commission of Science and Technology.

Supplementary Material Available: Tables of crystallographic data, H atom parameters, anisotropic thermal parameters, and bond distances and angles for the PF_6 groups (5 pages); table of observed and calculated structure factors for **1** (40 pages). Ordering information is given on any current masthead page.

(52) The energetics and intensities of the CT spectra in the $A_5Ru^{II}S(CH_3)_2$ complex are sensitive to the ionization potential assigned to the S(3d) orbitals. The mixing of S(d) orbitals into the frontier orbitals appears larger at the semiempirical INDO/S level than at the ab initio level.

(53) Krogh-Jespersen, K., to be submitted for publication.

(54) Rendell, A. P. L.; Bacskay, G. B.; Hush, N. S. *J. Am. Chem. Soc.* **1988**, *110*, 8343.

(55) Beratan, D. N.; Hopfield, J. J. *J. Am. Chem. Soc.* **1984**, *106*, 1584.